The interaction of oxygen molecules with iron films studied with MIES, UPS and XPS

K. Volgmann [a], F. Voigts [a], W. Maus-Friedrichs [a,b,*]

[a] Institut für Physik und Physikalische Technologien, Technische Universität Clausthal, Leibnizstrasse 4, 38678 Clausthal-Zellerfeld, Germany
[b] Clausthaler Zentrum für Materialtechnik, Leibnizstrasse 4, 38678 Clausthal-Zellerfeld, Germany

ARTICLE INFO

ABSTRACT

X-ray Photoelectron Spectroscopy (XPS), Metastable Induced Electron Spectroscopy (MIES) and Ultraviolet Photoelectron Spectroscopy (UPS) were applied to study the interaction of oxygen molecules with iron films. Supplementarily, iron oxide was investigated for comparison.
With XPS from the Fe $2p_{3/2}$ range contributions of metallic Fe as well as Fe^{2+} and Fe^{3+} can be distinguished. During the interaction with oxygen an oxide film is formed on the iron surface. Nevertheless, XPS still shows metallic contributions even for a surface which is saturated with more than 10^4 L. The oxide film hinders the dissociation of further impinging oxygen molecules.
The interaction of He* atoms with iron oxide surfaces during MIES is dominated by Auger Neutralization. This surprising result follows from the high work function and the fact that intrinsic defects result in a Fermi level pinning to the conduction band.

© 2010 Elsevier B.V. All rights reserved.

1. Introduction

Iron is a widely used material. Beside all technological applications a rather new point of interest is the occurrence of iron and its oxides on our neighbor planet Mars. Its core is mainly made up of iron and its surface consists partly of the minerals hematite and goethite. These two minerals are thought to be formed only in the presence of water which was also found either as ice or even in liquid phase [1,2]. In Mars' atmosphere which mainly consists of CO_2, traces of methane (10 ppb) and formaldehyde (100 ppb) are found [3,4]. These two gases lead to a discussion about their origin. On the one hand a biological origin is proposed [5,6] as methane is possibly produced by fermentation. On the other hand non-biological chemical reactions are argued to be the origin [7–9]. We found in a preliminary experiment that methane and formaldehyde are formed under near Martian conditions on hematite due to a photocatalytic reaction [10]. Because such reactions depend strongly on the surface properties we try to create a basis data set for iron oxides to allow further investigations. This is the main aim of this work.

Most investigations on iron oxides and the oxide formation applied core level photoelectron spectroscopy [11–15] and valence band photoelectron spectroscopy [12–14,16]. These investigations mostly regarded the different types of iron oxides, but only less the fundamental interaction between oxygen and iron. MIES results shown here are not available up to now.

One scope of this paper is therefore the analysis of the surface reaction between iron and oxygen under controlled vacuum conditions. We used Metastable Induced Electron Spectroscopy (MIES), Ultraviolet Photoelectron Spectroscopy (UPS) and X-ray Photoelectron Spectroscopy (XPS). In a forthcoming paper we will present results of the interaction of iron and iron oxides films with H_2O, CO and CO_2. Additionally the origin of methane and its possible formation under Martian conditions on hematite and goethite surfaces will be a focus of our future work.

2. Experimental

2.1. Setup and analysis

An ultrahigh vacuum apparatus with a base pressure of $5 \cdot 10^{-11}$ mbar, which has been described in detail previously [17], is used to carry out the spectroscopic measurements.

Electron spectroscopy is performed using a hemispherical analyzer (VSW HA100) in combination with a source for metastable helium atoms (He*) and ultraviolet photons (HeI line). A commercial non-monochromatic X-ray source (Specs RQ20/38C) is utilized for XPS.

During XPS, X-ray photons hit the surface under an angle of 80° to the surface normal, illuminating a spot of several mm in diameter. For all measurements presented here, the Al K_α line with a photon energy of 1486.7 eV is used. Electrons are recorded by the hemispherical analyzer with an energy resolution of 1.1 eV under an angle of 10° to the surface normal. All XPS spectra are displayed as a function of binding energy with respect to the Fermi level.

For quantitative XPS analysis, photoelectron peak areas are calculated after background correction. Especially the strong increase

of the inelastic background at the Fe 2p signal has to be corrected with either the method of Tougaard [18] or Shirley [19]. We use the Shirley Method as we achieve the most consistent stoichiometric results for our measurements with it. Peak fitting with Gauss-type profiles was performed using OriginPro 7G including the PFM fitting module which uses Levenberg–Marquardt algorithms to achieve the best agreement possible between experimental data and fit.

Photoelectric cross-sections as calculated by Scofield [20] and inelastic mean free paths from the NIST database [21] as well as the transmission function of our hemispherical analyzer are taken into account when calculating stoichiometry. Essentially, the peak fitting procedure is done as described in [17]. To find suitable fitting parameters consistent with the stoichiometry of the iron oxide we followed the pathway proposed by Lin et al. [11]:

1. Fitting of the Fe $2p_{3/2}$ peak of the clean iron film. This delivers the Full Width at Half Maximum (FWHM) of the metallic contribution in the Fe $2p_{3/2}$ peak. It is denoted as Fe^0 oxidation state in the following.
2. Peak fitting of Fe $2p_{3/2}$ and O 1s of the iron oxide film on the basis of the known stoichiometry. This delivers the FWHM of the Fe^{3+} oxidation state's contribution in the Fe $2p_{3/2}$ peak. It is referred to as Fe^{3+} in the following. This step also includes the comparison with the fitting results of the Fe $2p_{3/2}$ and O 1s of iron oxide powder. A contribution by the Fe^{2+} oxidation state is taken into account basing on literature and results for the iron oxide powder.
3. Iterative repeating of steps 1 and 2. Constraints are the FWHM and the relative energetic distances of Fe $2p_{3/2}$ and O 1s. These values have to match each other and the literature consistently.
4. Peak fitting of the Fe $2p_{3/2}$ of the iron oxide film delivers the Fe^{2+} and Fe^{3+} peak contributions, their relative energetic distances among each other and the relative energetic distances to the metallic contribution. This delivers a complete basic data set for the following analysis of oxygen covered iron films.

Our experimental experience and the good reproducibility of the experiments allow us to estimate the typical deviation in our results to be certainly below 10%.

MIES and UPS are performed by applying a cold cathode gas discharge via a two-stage pumping system. A time-of-flight technique is employed to separate electrons emitted by He* interaction (MIES) from those caused by HeI interaction (UPS) with the surface. The mixed He*/HeI beam strikes the sample surface under an angle of 45° to the surface normal and illuminates a spot of approximately 2 mm in diameter. The spectra are recorded simultaneously by the hemispherical analyzer with an energy resolution of 220 meV under normal emission within 280 s.

MIES is an extremely surface sensitive technique probing solely the outermost layer of the sample, because the He* atoms interact with the surface typically 0.3 to 0.5 nm in front of it. This may occur via a number of different mechanisms depending on surface electronic structure and work function, as is described in detail elsewhere [22,23]. On pure and partly oxidized metal surfaces Auger Neutralization (AN) occurs as long as the surface shows metallic behavior. As a result the impinging He* atom is ionized in the vicinity of the surface by resonant transfer (RT) of its 2s electron in unoccupied metallic surface states. Afterwards, the remaining He^+ ion is neutralized by a surface electron thus emitting a second surface electron carrying the excess energy. The observed electron spectrum is rather structureless and originates from a self convolution of the surface density of states (SDOS). On large band gap oxides and low work function metals Auger Deexcitation (AD) takes place. During Auger Deexcitation an electron from the sample fills the 1s orbital of the impinging He*. Simultaneously, the He 2s electron is emitted carrying the excess energy. The resulting spectra reflect the surface density of states directly. AD-MIES and UPS can be compared and allow a distinction between surface and bulk contributions.

All MIES and UPS spectra are displayed as a function of the electron binding energy with respect to the Fermi level. The surface work function can be determined from the high binding energy onset of the MIES or the UPS spectra with an accuracy of ± 0.1 eV.

2.2. Sample preparation

Iron films were prepared by evaporating iron (Goodfellow, 99.95% pure) with a commercial UHV evaporator (Omicron EFM3) onto a tungsten foil with 0.2 mm thickness (PLANSEE Composite Materials GmbH, 99.97% pure). The W target is cleaned from surface contaminations by heating to approximately 1425 K prior to deposition. Iron is subsequently offered at a rate of 0.35 nm/min for 45 min at room temperature. This procedure results in an iron film of about 16 nm thickness as estimated from preliminary XPS measurements. XPS data of freshly prepared iron films are generally showing little surface contaminations, only an O 1s signal corresponding to a fraction of about 10 at.% can be detected. Sputtering of a freshly prepared iron film reduces this contamination. Neither in MIES/UPS nor in XPS can any signal due to the W substrate be detected for an iron film of this thickness.

Iron oxide films were prepared step by step applying the following procedure being performed at a sample temperature of 725 K following the scheme proposed by Ranke and Weiss [12]:

1. Heating the sample to 725 K.
2. Evaporation of iron at a rate of 0.35 nm/min for 20 min.
3. Oxidation of this thin iron layer at an oxygen partial pressure of $2.7 \cdot 10^{-7}$ mbar for 10 min (corresponding to an exposure of 120 L).
4. Evaporation of iron at a rate of 0.35 nm/min in an oxygen atmosphere of $2.7 \cdot 10^{-7}$ mbar for 10 min.
5. Further oxidation of this iron oxide layer at an oxygen partial pressure of $2.7 \cdot 10^{-7}$ mbar for 10 min.
6. Repeating of steps 3 and 4 for a second time.
7. Final oxygen offer at a partial pressure of $2.7 \cdot 10^{-7}$ mbar for 5 min.
8. Cooling down of the sample to room temperature.

The resulting iron oxide film thickness is about 10 nm. This is calculated from the W 4f attenuation. Important for this calculation is the use of the inelastic mean free path for electrons in Fe_2O_3 using the NIST Electron IMFP database [21].

The iron oxide film thickness calculated in this manner does not account for a mixture of several different oxidation states of iron. Therefore this is an estimate unless the preparation procedure ensures the growth of a homogeneous Fe_2O_3 layer as described in [12,24]. To distinguish this film clearly from the oxygen saturated iron film discussed later it is denoted as iron oxide film in the following.

The sample of Fe_2O_3 powder (Sigma-Aldrich, <5 μm, 99+% pure) was prepared by pressing with 300 bar. An amount of approximately 100 mg Fe_2O_3 powder was compacted to a disc (thickness about 500 μm) with a diameter of 14 mm in a molybdenum sample holder. After the ex-situ preparation the sample was heated to 670 K in UHV. Subsequently, it was annealed at 500 K at an oxygen pressure of $1.2 \cdot 10^{-7}$ mbar for 120 min, corresponding to an exposure of 630 L. This sample is referred to as *iron oxide powder* in the following.

O_2 is offered via backfilling the chamber using a bakeable leak valve. The gas line is evacuated and can be heated in order to ensure cleanness. Additionally, a cryo trap is installed to minimize water contamination during oxygen exposure. A quadrupole mass spectrometer (Balzers QMS 112A) is used to monitor the partial pressure of the reactive gases during experiments simultaneously to MIES and UPS measurements. Very high oxygen exposures are offered in a high pressure cell attached to the UHV apparatus via a transfer system. It employs the same gas line as described above. The iron film which has been exposed to O_2 is denoted as *oxygen saturated iron film*.

3. Results and discussion

The interpretation of XPS data for iron during its oxidation is quite complicated due to a large number of possible oxidation states and corresponding shake-up peaks as well as the Fe 2p spin-orbit splitting. Therefore we start our investigation with a fundamental analysis of pure iron and well-defined iron oxide. Thus we follow the guideline for a consistent quantitative XPS peak analysis published by Lin et al. [11]. Afterwards we will discuss our results for the interaction of oxygen with Fe films basing on this analysis.

3.1. Basic investigations on iron and iron oxide

Fig. 1a shows an XPS survey spectrum of the iron film. After preparation XPS shows an oxygen contribution (O 1s peak at a binding energy of 531 eV) due to unavoidable contamination from the evaporator (not shown here). To clean the iron film surface, the sample is sputtered for 3 min (3 kV discharge voltage, 5 mA emission current and $5 \cdot 10^{-6}$ mbar Argon partial pressure corresponding to a sputter rate of approximately 0.3 nm/min). After sputtering the amount of oxygen at the sample surface is lowered, but the signal does not vanish completely, as can be seen in Fig. 1a. The O 1s peak
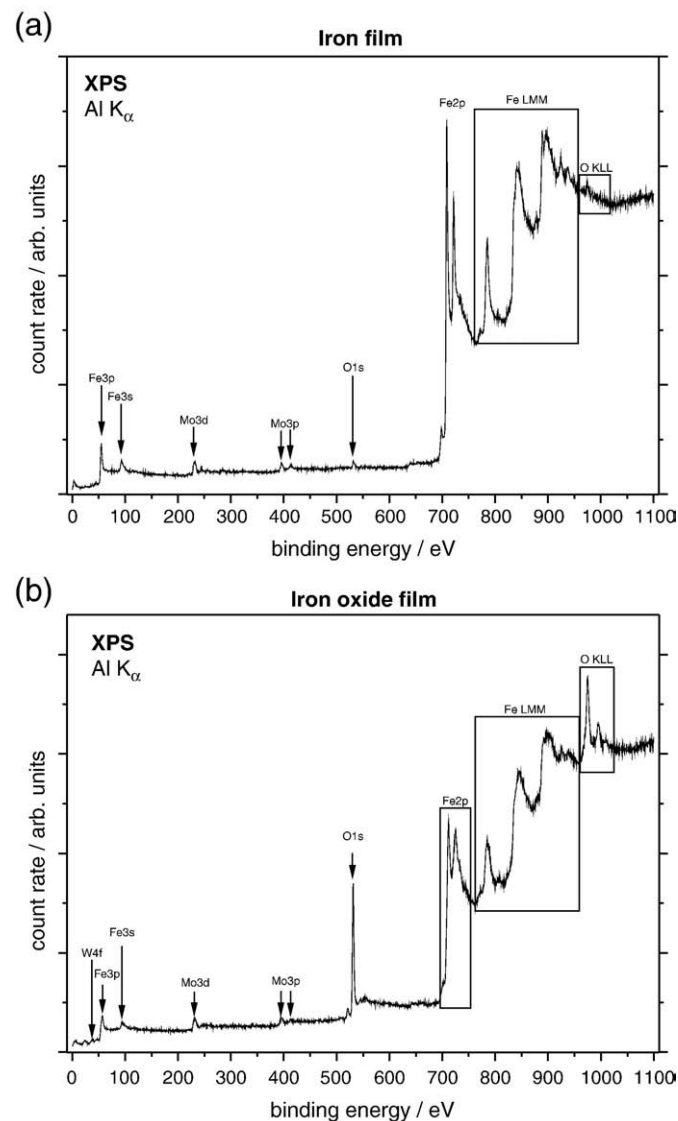
contribution to global stoichiometry is about 10 at.%. We calculate that the top layer contributes to the complete XPS signal by about 17%. Assuming that all oxygen atoms would be located in the top iron layer we find that the top surface layer should include about 60% oxygen atoms. We will show MIES and UPS spectra of this pure iron film (Fig. 5) which do not show any comparable oxygen contribution. It is therefore concluded, that the observed oxygen atoms are dissipated in the iron film. The most significant feature in this spectrum is the Fe 2p signal. Iron has a large spin-orbit splitting of about 13 eV. For the following evaluations and discussion, only the Fe $2p_{3/2}$ contribution (binding energy range 705–720 eV) is fitted and analyzed. Fe 3p and Fe 3s signals cannot be interpreted and discussed in a comparable simple way, as already mentioned in previous works [13–15]. Also visible in the XPS spectrum are two molybdenum signals (Mo 3p and Mo 3d). These contributions stem from the sample holder and do not influence our discussions. Detailed analysis of the relevant peaks is done with Fig. 2.

Fig. 1b shows the XPS survey spectrum of the iron oxide film. The film was produced as described in Section 2.2. The iron oxide film thickness is about 10 nm as estimated from the W 4f signal attenuation. Both XPS survey spectra in Fig. 1 show the Auger lines Fe LMM and O KLL. A detailed analysis of the relevant peaks is shown in Fig. 3.

Fig. 2 shows the Fe 2p range of a XPS analysis of the iron film. For stoichiometry evaluation only Fe $2p_{3/2}$ is analyzed. The fitting procedure results in three sub-peaks. The original data are shown as dots, the green lines represent the three sub-peaks and the red line shows the sum of all sub-peaks. The signal of the metallic contribution (denoted by Fe^0) is found at the low binding energy side at 707.8 eV with a FWHM of 2.27 eV. Its binding energy differs up to 1 eV from literature [11,13,14] for all measurements. As can be seen in Table 1, this is a constant offset which we find for all peaks. It has its origin in the fact that we do not correct our binding energy scale to a reference peak. This is acceptable, as we interpret and discuss relative energies only. The Fe^0 FWHM is fixed to 2.27 eV in all following data fits, because no influence from other species can occur which would disturb Fe^0. All evaluated FWHMs and binding energies of all measurements are collected in Table 1. The signal of the Fe^{2+} peak contribution is observed at 710.0 eV. It provides a FWHM of 1.67 eV. The energetic distance between Fe^0 and Fe^{2+} amounts to 2.3 eV. At the high binding energy shoulder between the Fe $2p_{3/2}$ and Fe $2p_{1/2}$ main contributions a third peak is found at about 715 eV. It is a well

Fig. 1. XPS survey spectra of an iron film (thickness approximately 16 nm) (a) and an iron oxide film (thickness approximately 10 nm) (b).
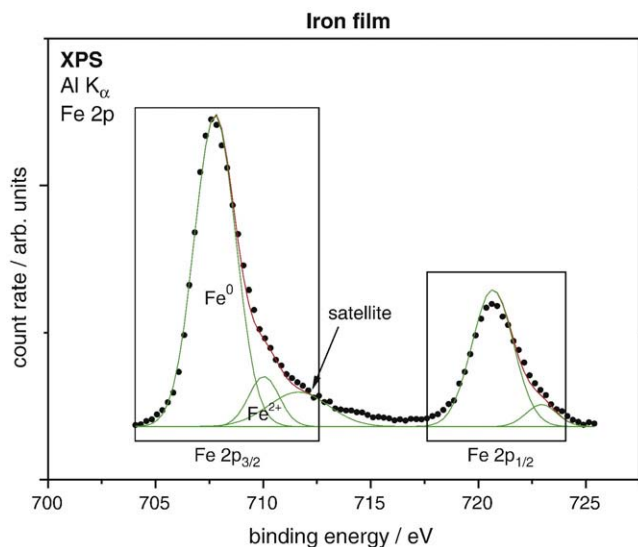

Fig. 2. XPS detail spectra of the Fe 2p region of the iron film shown in Fig. 1. For preparation details see Section 2.2. The highlighted Fe $2p_{3/2}$ section is used for analysis only, as this is done also for Figs. 4 and 7.
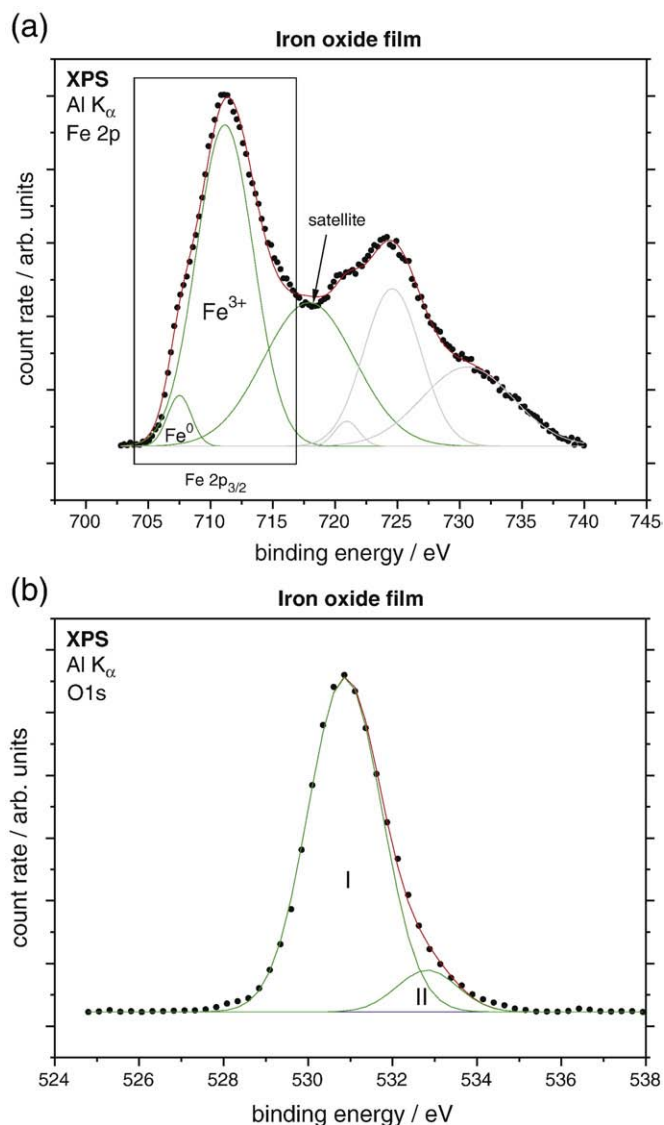
Fig. 3. XPS detail spectra of Fe 2p (a) and O 1s (b) of the iron oxide film (produced at a sample temperature of 725 K, at an oxygen partial pressure of $2.7 \cdot 10^{-7}$ mbar and iron evaporation rate of 0.35 nm/min).

known satellite which was identified as a Fe^{2+} contribution [11,13,14]. Up to now, it is not clear what kind of satellite this peak represents. Carlson [25] discussed this structure in detail and states that it is produced by a shake-up process. In contrast, McIntyre et al. [13] found a low probability for this shake-up process. They favor a multiplet splitting which is induced by the interaction of the remaining core after the photoionization process with the ligand states. This is supported by a recent discussion of Paparazzo [26]. A comparable multiplet splitting was found with MIES and UPS for NiO [27,28] and CoO films [29]. Nevertheless, for the results presented and discussed here it is only important, that the emission at 715 eV is induced by Fe^{2+} states and does neither occur for Fe^0 nor for Fe^{3+}.

Fig. 3a displays the Fe 2p detail spectrum of the iron oxide film. The signal of Fe^0 is found at a binding energy of 707.5 eV. A second peak is found at a binding energy of 711.1 eV. This peak is due to the occurrence of iron(III) oxide (denoted as Fe^{3+}) [11,13–15]. The energetic distance between Fe^0 and Fe^{3+} amounts to 3.6 eV. The absence of any Fe^{2+} contribution and the $O{:}Fe^{3+}$ ratio of 1.85 are accounting for this conclusion. The ideal stoichiometric relation between oxygen and iron is 1.5. A higher oxygen proportion is possible due to the high oxygen offer during preparation, so it has to be suspected that the sample is slightly over-stoichiometric in oxygen. Another aspect to be kept in mind is mentioned by Lin et al. [11] who argued that atomic sensitivity factors (ASF) for example published in [30] are not accurate enough for a detail stoichiometry analysis. They obtained the ASF for their apparatus by measurement of iron oxide samples of known composition. We suspect that the used photoelectric cross-sections found in [20] also may be afflicted with a certain deviation. Due to this assumption we follow the argumentation by Lin et al. and compared our prepared iron oxide film with a reference Fe_2O_3 powder sample (see Fig. 4).

Fig. 3b shows the O 1s detail spectrum of the iron oxide film. It consists of two contributions. The signal at 530.9 eV (denoted by O 1s I) is assigned to the oxygen forming the iron oxide. As mentioned already in the discussion of Fig. 3a, the discrepancy in the binding energy compared to literature is also found here. Nevertheless, the relative energetic distance between e.g. the Fe^0 and the O 1s I peaks is the same as found in the literature. For the iron oxide film we find 176.6 eV which is close to a literature value of 176.5 eV [11,13]. The second peak at the high binding energy shoulder is denoted by O 1s II. Yet, the origin of this second contribution is not clear. In literature, this contribution is frequently referred to as a chemisorbed OH [11,13]. Its relative energetic distance to the first contribution is reported between 1.1 eV and 1.7 eV, while we observe a value of 1.95 eV. Additional measurements with MIES and UPS (not shown here)

Table 1
Summarized values of all XPS measurements (q, p denote the valency; $p = 0, 2+, q = 2+, 3+$).

System	Figure	Peak	Fe 2p		O 1s		Assignment	$\Delta E(Fe^p - Fe^q)$	Stoichiometry	d [nm]
			Energy	FWHM	Energy	FWHM			O/Fe^q	
Iron film	2	I	707.76	2.27			Fe^0		0.99	16.0
		II	710.03	1.67			Fe^{2+}	2.3		
		I			530.81	1.94	Oxide			
		II			532.60	3.84	Adsorbate			
Iron oxide film	3	I	707.50	2.27			Fe^0	3.6	1.85	9.6
		II	711.14	5.39			Fe^{3+}			
		I			530.87	2.05	Oxide			
		II			532.82	1.69	Adsorbate			
Iron oxide powder	4	I	715.40	4.89			Fe^{2+}	0.9	1.71	–
		II	716.32	4.89			Fe^{3+}			
		I			535.10	1.91	Oxide			
		II			536.00	3.90	Adsorbate			
Oxygen saturated iron film	7	I	707.41	2.27			Fe^0		1.82	–
		II	710.01	5.43			Fe^{2+}	2.6		
		III	711.01	5.43			Fe^{3+}	3.6		
		I			530.80	2.05	Oxide			
		II			532.80	2.33	Adsorbate			

(a)

Iron oxide powder

XPS
Al K$_\alpha$
Fe 2p

satellite

Fe^{3+}

Fe^{2+}

Fe 2p$_{3/2}$

binding energy / eV

count rate /arb. units

(b)

Iron oxide powder

XPS
Al K$_\alpha$
O 1s

I

II

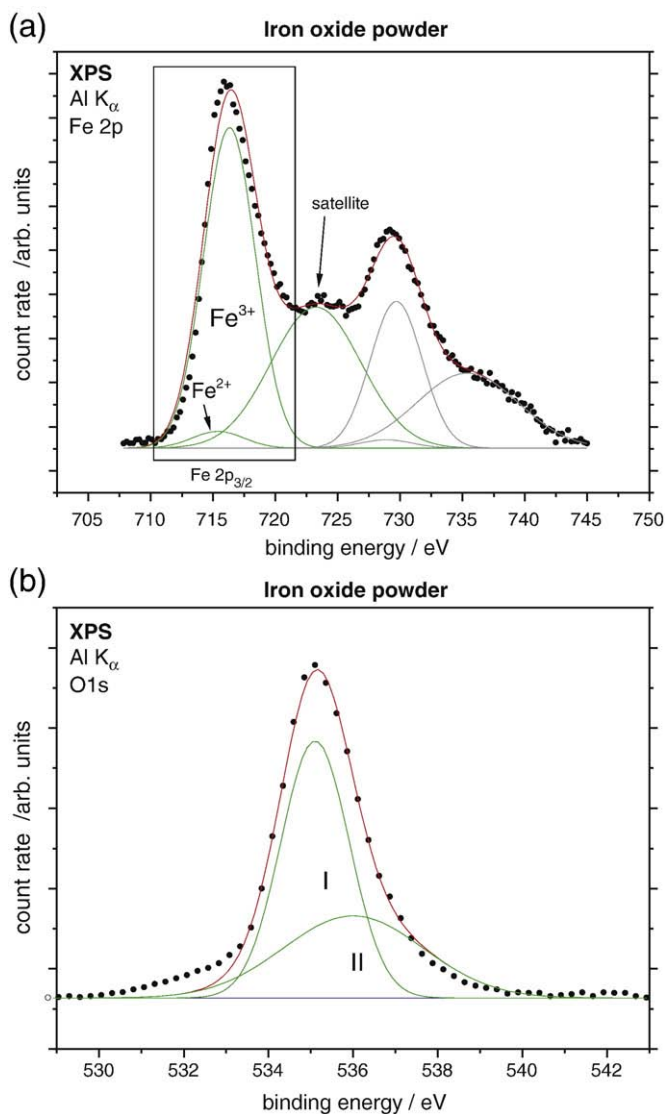binding energy / eV

count rate /arb. units

Fig. 4. XPS detail spectra of the Fe 2p (a) and O 1s regions (b) of iron oxide powder. For preparation details see Section 2.2.

appear to counter the interpretation as adsorbed OH. Our experiments applying a deliberate water exposure to iron oxide films do neither show OH nor adsorbed H_2O, although MIES is extremely sensitive to surface OH groups. These results will be presented in a future contribution. We assume the O 1s II peak to originate from oxygen not well incorporated into the iron oxide thus bound weaker to the surface and being chemisorbed. Brundle et al. also mention that the observed peak contribution in the region around 531 eV may not only correspond to OH. They refer to this contribution as "non-stoichiometric surface oxygen atoms" [14]. Our findings do support this picture.

Fig. 4a shows the Fe 2p detail spectrum of the Fe_2O_3 powder sample. Comparing this result with our in-situ produced iron oxide film (see Fig. 3a) it is evident that the produced iron oxide film is an iron(III) oxide film. Binding energy positions, FWHM and stoichiometry fit very well to each other. This may be seen clearly in Table 1. In contrast to the film, the powder sample shows no metallic contribution at a 3.6 eV lower binding energy compared to the Fe^{3+} contribution. Only a slight Fe^{2+} signal appears 0.9 eV below the main Fe^{3+} peak. Since we analyzed a powder sample, a charging of the oxide surface was unavoidable due to its thickness of about 500 μm. This charging amounts to approximately 5 eV.

Fig. 4b presents the O 1s detail spectrum of the Fe_2O_3 powder sample. Comparing it to Fig. 3b we find a much larger quantity of the O 1s II signal. The Fe_2O_3 sample was produced by pressing Fe_2O_3 powder particles as described in Section 2.2. The mean particle size is below 5 μm. The sample is porous and therefore provides a large surface. We suggested already with Fig. 3b, that O 1s II might be due to chemisorbed oxygen, which is not incorporated into a stoichiometric oxide. The observation that the surface increase results in an increase of O 1s II strongly supports this assumption. Both O 1s I contributions in Fig. 3a and Fig. 4a show the same FWHM.

3.2. Interaction of iron with oxygen

Fig. 5a shows MIES spectra obtained during the interaction of oxygen with the Fe film. These spectra were recorded at room temperature. The spectra are displayed cascaded as a waterfall graph. The bottom spectrum shows a typical Auger Neutralization process for a clean iron surface. With increasing oxygen offer, the peak of secondary electrons increases and the shoulder around 5 eV which is due to Auger Neutralization from Fe 3d states vanishes. To achieve oxygen saturation the sample is transferred to the adapted high pressure chamber after an exposure of 340 L. Therein it was exposed to further $2.71 \cdot 10^4$ L ($1 \cdot 10^{-5}$ mbar oxygen partial pressure for 60 min) of oxygen. A small peak around 5 eV arises which is due to O 2p electrons observed by the Auger Deexcitation process although the spectrum is mostly still due to the Auger Neutralization process. The O 2p peak must be due to Auger Deexcitation because the corresponding UPS spectra (see Fig. 5b) show the same peak at this energetic position. The work function of the oxygen saturated Fe film is found to be 4.6 eV.

For MIES investigations of NiO(100) surfaces it was observed by Morgner [23], that Ni 3d orbitals are strongly localized at the Ni^{2+} atoms, therefore Ni 3d orbitals were only weakly visible although the spectrum was completely due to an Auger Deexcitation process. We assume that this similarly holds for Fe 3d orbitals in Fe^{3+} and probably Fe^{2+}. Therefore the resonant transfer process into unoccupied orbitals, preceding the Auger Neutralization process, does not dominate the interaction completely. The He*–surface interaction on this surface may occur via resonant transfer including unoccupied Fe 3d orbitals and subsequent Auger Neutralization or via Auger Deexcitation including O 2p orbitals. It is pretty surprising to find MIES spectra from insulators which are not dominated by Auger Deexcitation. It is usually assumed that on insulating surfaces Auger Neutralization should not be possible. Obviously, we find that the He*–surface interaction does not follow the simple picture, that oxides generally show Auger Deexcitation processes. This may be understood taking into account, that the large work function of the iron oxide plays an important role.

The energy scheme of the Auger Neutralization process is shown in Fig. 6. In the first step, an electron from the He 2s level is transferred into unoccupied states in the conduction band via a resonant transfer process. This is possible, because the work functions of the samples are large enough. We find a work functions of 4.6 eV for the oxygen saturated iron film. The He 2s level is known to be 4.77 eV below the vacuum level and we may expect a rise in front of the surface due to image charge effects [23]. From the MIES spectrum we find a gap of 2.2 eV between valence band maximum and the Fermi level. This resembles the well known band gap of Fe_2O_3 which amounts 2.2 eV, too [31]. Therefore we conclude that the Fermi level is pinned to the conduction band minimum due to intrinsic defects. This means that the He* 2s electrons come in resonance with unoccupied states from Fe 3d orbitals at the surface which results in a very high probability for the resonant transfer of these electrons.

Fig. 5b illustrates the corresponding UPS spectrum. The bottom spectrum shows the clean iron film, which is, beside the secondary electrons, dominated by the Fe 3d emission just below the Fermi level
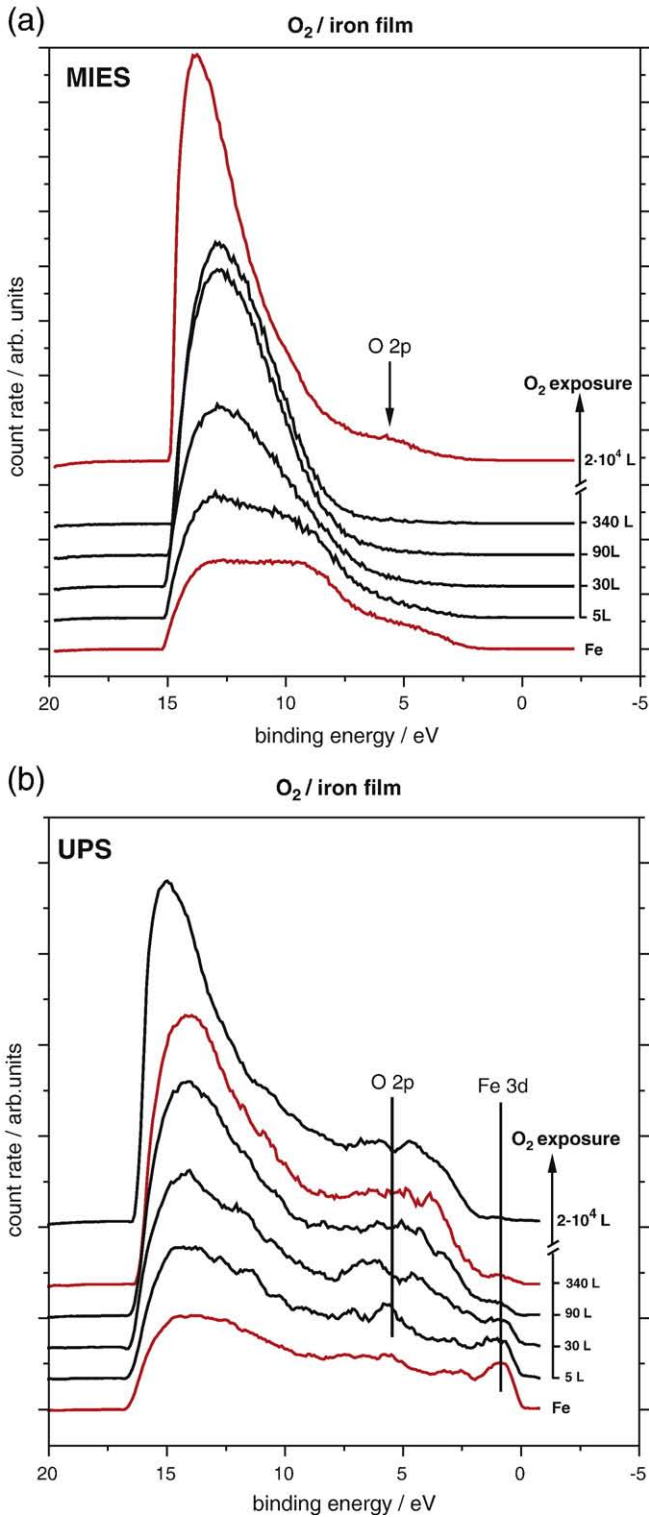
(a) O₂ / iron film

(b) O₂ / iron film

Fig. 5. MIES and UPS spectra during oxygen offer to the iron film. The top spectrum corresponds to a final oxygen offer of $2.71 \cdot 10^4$ L and matches the spectra in Fig. 7.

Fig. 6. Schematic energy scheme and interaction processes of He* with an iron oxide surface. RT denotes the resonant transfer, AN means Auger Neutralization, and VB stands for valence band as CB for conduction band.

at 1 eV. This is in agreement with the literature [14,25]. With increasing oxygen offer, the Fe 3d signal decreases and a significant contribution due the O 2p arises at 5.6 eV. As mentioned above in the description of Fig. 1a, an O 1s signal is found in the XPS survey spectrum. This oxygen proportion does not accumulate in the topmost layer, because the MIES and UPS spectra of the clean iron film do not show any O 2p 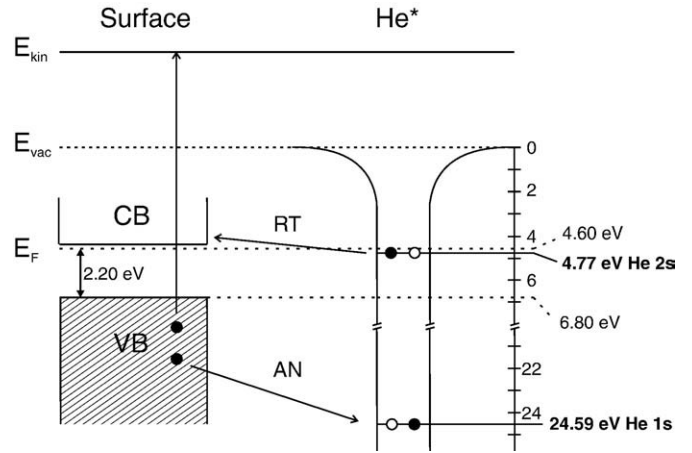contribution. Thus we assume that the oxygen is distributed homogenously within the bulk. The top UPS spectrum of the completely oxygen saturated surface is very similar to the UPS spectrum of the iron oxide sample (not shown here). It is also in accordance to literature [12,16,25].

Fig. 7a displays the XPS detail spectrum of the Fe 2p of the oxygen saturated iron film (corresponding to the top spectrum in Fig. 5). The relative energetic distances between Fe^0, Fe^{2+} and Fe^{3+} from Figs. 3 and 4 as well as the FWHM of Fe^0 from Fig. 2 are fixed as constraints for the fit. The most significant contribution is Fe^{3+} at a binding energy of 711.0 eV. Only a small amount of Fe^{2+} is observed whereas a significant Fe^0 signal is found at a binding energy of 707.4 eV. This fit provides the best agreement with the experimental data. All other fits allowing a bigger Fe^{2+} contribution show larger deviations between data and fit. Nevertheless, the differences between deviations from varying fits are quite small. Therefore, a Fe^{2+} contribution up to 20% of the Fe^{3+} cannot be excluded from our data.

Although the spectra are recorded after the additional preparation in the high pressure chamber, there still remains some metallic iron. While iron is known to be very corrosive under ambient atmosphere, we do not achieve a complete oxidation during the interaction with sheer oxygen. The sticking coefficient of oxygen molecules adsorbing on iron is zero as the coverage of $2.1 \cdot 10^{15}$ cm^{-2} is reached [32]. At this exposure a passivating oxide film is formed on top of the surface. Further impinging oxygen molecules cannot be dissociated due to the lack of charge density near the Fermi level. Therefore no oxygen atoms can be provided to enlarge the oxide layer. Further impinging oxygen molecules are reflected without interaction. This behavior is similar to the passivation of aluminium by an oxide film [33]. Because of this, thick iron oxide films may only be grown by the method described in Section 2.2.

Fig. 7b shows the XPS detail spectrum of the O 1s of the oxygen saturated iron film. Two contributions are visible similar to Figs. 3b and 4b at binding energies 530.5 eV and 532.3 eV. The calculated stoichiometry for this oxygen saturated iron film leads to an O:Fe^{3+} ratio of 1.82. The composition of the oxygen saturated iron film seems to be over-stoichiometric concerning the O 1s I contribution compared to the Fe^{3+} contribution, e.g. the film contains too much oxygen. As it is not possible to distinguish qualitatively and quantitatively between different oxidation states within the O 1s I contribution with XPS using our setup, no information on the amount of oxygen bound to Fe^{3+} or Fe^{2+} states can be found. The uncertainty amounts to about 10% as already mentioned in Section 2.2. Following this O:Fe^{3+} ratio we conclude that predominantly iron(III) oxide is formed.
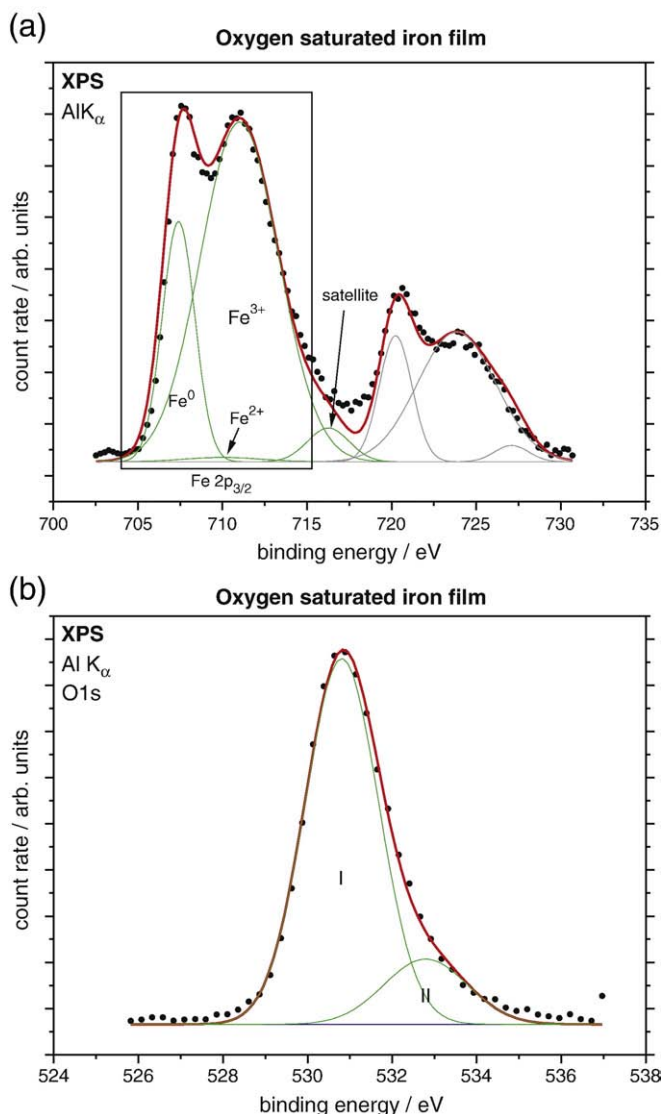
Fig. 7. XPS detail spectra of Fe 2p (a) and O 1s (b) of the oxygen saturated iron film (exposed to $2.71 \cdot 10^4$ L oxygen) corresponding to the top spectra in Fig. 5.

We want to emphasize at this point that the O 1s II contribution at the high binding energy side of the O 1s peak does not account for adsorbed OH groups as often announced in older work, see for example [11,15]. Our MIES and UPS spectra do not show any OH contributions, although MIES is known to be extremely sensitive for adsorbed OH groups [34,35]. MIES shows only O 2p emission from the oxide, meaning that even the topmost layer does not show any adsorbed OH groups. Adsorbed OH would display a well known peak doublet [34,35], which is not observed here. We therefore conclude that the secondary contribution at the high binding energy side of the O 1s peak does not account for OH groups. The common assumption of OH adsorption due to a residual water content in any UHV chamber or water contamination in the offered O_2 does not seem to hold. This is in agreement with Brundle et al. [14] as has been discussed already with Fig. 3b.

4. Summary

Iron and iron oxide films are produced and investigated by XPS, MIES and UPS. Both samples, iron oxide films and oxygen saturated iron films, consist mainly of iron(III) oxide as confirmed by comparing XPS measurements with a powder Fe_2O_3 reference sample.

UPS measurement of the clean iron film shows a metallic behavior dominated by the Fe 3d just below the Fermi level. These contributions decrease during oxygen exposure while the O 2p emission is increasing accordingly. This indicates the conversion to an iron oxide as the signal from a Fe 3d contribution near the Fermi level vanishes.

MIES of a clean iron film indicate the well known Auger Neutralization process. Surprisingly, the interaction process does not change due to the ongoing formation of the iron oxide film. Only at the very high oxygen exposure beyond 10^4 L we observe Auger Deexcitation from O 2p orbitals. Thus both Auger Neutralization and Auger Deexcitation concurrence and due to the high work function of the iron oxides and the Fermi level pinning to the conduction band minimum the Auger Neutralization process appears to be more probable.

In XPS, a significant signal contribution belonging to metallic iron is still found even after a saturation oxygen offer. This is also observed in UPS. We find that the top iron oxide is forming a passivating layer which is shown by the strongly reduced intensity beyond the Fermi level. This layer would not inhibit oxygen atom diffusion but inhibits the dissociation of impinging oxygen molecules, which most likely will be repelled without any surface interaction. Therefore, the lack of oxygen atoms on the surface is the reason for the incomplete surface layer oxidation.

The combination of MIES, UPS and XPS for oxygen saturated iron films shows very clearly that no OH groups are formed due to the residual water atmosphere. The XPS O 1s high binding energy feature, up to now mostly attributed to adsorbed OH, is therefore assumed to be due to chemisorbed oxygen which is not incorporated into a stoichiometric oxide.

References

[1] D. Möhlmann, Astrobiology 5 (2005) 770.
[2] T. Dambeck, Wasser auf dem Mars, Spektrum der Wissenschaft, Dossier 3, Der Mars (2004) 78.
[3] V. Formisano, et al., Science 306 (2004) 1758.
[4] Th. Encrenanz, et al., Planet. Space Sci. 52 (2004) 1023.
[5] H.P. Klein, et al., Science 194 (1976) 99.
[6] V.A. Krasnopolsky, et al., Icarus 172 (2004) 537.
[7] J.R. Lyons, C.E. Manning, F. Nimmo, Geophys. Res. Lett. 32 (2005) L13201, doi:10.1029/2004GL022161.
[8] A. Bar-Nun, V. Dimitrov, Icarus 181 (2006) 320.
[9] C. Oze, M. Sharma, Geophys. Res. Lett. 32 (2005) L10203.
[10] B. Roos, D. Schwendt, Extraterristrische Chemie, student research project, Institute of Physics and Physical Technologies, Technical University Clausthal, 2006.
[11] T.-C. Lin, G. Sehadri, J.A. Kelber, Appl. Surf. Sci. 119 (1997) 83.
[12] W. Ranke, W. Weiss, Prog. Surf. Sci. 70 (2002) 1.
[13] N.S. McIntyre, D.G. Zetaruk, Anal. Chem. 49 (1977) 1521.
[14] C.R. Brundle, T.J. Chang, K. Wandelt, Surf. Sci. 68 (1977) 459.
[15] T. Yamashita, P. Hayes, Appl. Surf. Sci. 254 (2008) 2441.
[16] V.E. Henrich, P.A. Cox, The Surface Science of Metal Oxides, Cambridge University Press, 1994.
[17] M. Frerichs, F. Voigts, W. Maus-Friedrichs, Appl. Surf. Sci. 253 (2006) 950.
[18] S. Tougaard, Pract. Surf. Sci. 216 (1989) 343.
[19] D.A. Shirley, Phys. Rev. B 5 (1972) 4709.
[20] J.H. Scofield, J. Electron Spectrosc. Relat. Phenom. 8 (1976) 129.
[21] National Institute of Standards and Technology Electron Inelastic-Mean-Free-Path Database 1.1, <http://www.nist.gov/srd/nist71.htm>, last accessed: March 2010.
[22] Y. Harada, S. Masuda, H. Ozaki, Chem. Rev. 97 (1997) 1897.
[23] H. Morgner, Adv. At. Mol. Opt. Phys. 42 (2000) 387.
[24] Joseph, Y. Spektroskopische Untersuchungen zur Oberflächenchemie von einkristallinen Eisenoxidfilmen, Dissertation Freie Universität Berlin 2001.
[25] T.A. Carlson, Discuss. Faraday Soc. 60 (1975) 30.
[26] E. Paparazzo, J. Electron Spectrosc. Relat. Phenom. 154 (2006) 38.
[27] H. Morgner, Adv. At. Mol. Opt. Phys. 42 (2000) 387.
[28] T. Kubiak, H. Morgner, O. Rakhovskaya, Surf. Sci. 321 (1994) 229.
[29] M. Frerichs, F.X. Schweiger, F. Voigts, S. Rudenkiy, W. Maus-Friedrichs, V. Kempter, Surf. Int. Anal. 37 (2005) 633.

[30] J.F. Moulder, W.F. Stickle, P.E. Sobol, K.D. Bomben, in: J. Chastian, R.C. King (Eds.), Handbook of X-ray Photoelectron Spectroscopy, Physical Electronics, Inc, Eden Prairie, Minnesota, 1995.

[31] R.M. Cornell, U. Schwertmann, The Iron Oxides: Structure, Properties, Reactions, Occurence and Uses, VCH, New York, 1996.

[32] T.-U. Nahm, R. Gomer, Surf. Sci. 373 (1997) 237.

[33] M. Frerichs, F. Voigts, W. Maus-Friedrichs, Appl. Surf. Sci. 253 (2006) 950.

[34] F. Bebensee, F. Voigts, W. Maus-Friedrichs, Surf. Sci. 602 (2008) 1622.

[35] W. Maus-Friedrichs, A. Gunhold, M. Frerichs, V. Kempter, Surf. Sci. 488 (2001) 239.